

RSC Advances



This is an *Accepted Manuscript*, which has been through the Royal Society of Chemistry peer review process and has been accepted for publication.

Accepted Manuscripts are published online shortly after acceptance, before technical editing, formatting and proof reading. Using this free service, authors can make their results available to the community, in citable form, before we publish the edited article. This *Accepted Manuscript* will be replaced by the edited, formatted and paginated article as soon as this is available.

You can find more information about *Accepted Manuscripts* in the [Information for Authors](#).

Please note that technical editing may introduce minor changes to the text and/or graphics, which may alter content. The journal's standard [Terms & Conditions](#) and the [Ethical guidelines](#) still apply. In no event shall the Royal Society of Chemistry be held responsible for any errors or omissions in this *Accepted Manuscript* or any consequences arising from the use of any information it contains.

Towards highly efficient photoanodes: The role of carrier dynamics on the photoelectrochemical performance of InGaN/GaN multiple quantum well coaxial nanowires

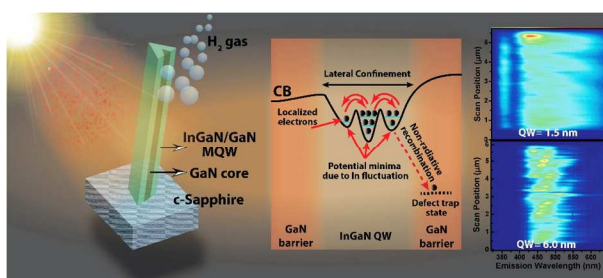
Mohamed Ebaid^{1,3}, Jin-Ho Kang¹, Seung-Hyuk Lim², Yong-Hoon Cho² and Sang-Wan Ryu^{1,*}

¹Department of Physics, Chonnam National University, Gwangju 500-757, Republic of Korea

²Department of Physics and KI for the NanoCentury, Korea Advanced Institute of Science and Technology, Daejeon 305-701, Republic of Korea

³Department of Physics, Faculty of Science, Beni-Suef University, Beni-Suef 62511, Egypt

Table of Contents



The carrier dynamics in highly active InGaN/GaN coaxial nanowire photoanodes were studied for photoelectrochemical water splitting applications that can provide deeper insight to enhance the photon-to-electron conversion efficiency.

*) sangwan@chonnam.ac.kr

The carrier dynamics in InGaN/GaN multiple quantum well coaxial nanowires (MQW-CNWs) with three different quantum well (QW) thicknesses and the same barrier thickness were studied optically using temperature-dependent and time-resolved photoluminescence spectroscopies. The role of the carrier dynamics on the photoelectrochemical water splitting (PEC-WS) performance of the MQW-CNWs was also investigated. The dependence of the PEC-WS performance and carrier dynamics on the QW thickness provided results indicative of the impact of the exciton localization and the defect states in the photoanodic performance of the MQW-CNWs. Strong localization effects and defect-induced recombination have been shown using samples with a thin QW with thicknesses up to 3 nm. During the PEC-WS, the samples showed a large onset potential and a low photocurrent density that led to low incident-photon-to-current conversion efficiency (IPCE). As the QW thickness approached 6 nm, negligible localization as well as improved photoemission quality were achieved, which lead to a small overpotential and a high IPCE of approximately 15%. The result demonstrated that the efficient photoanode requires a high crystal quality and weak localization, which can be achieved through the careful structural optimization.

Introduction

Solar photoelectrochemical water splitting (PEC-WS) using a semiconductor photoelectrode is a process in which the electron and the hole created by the absorption of solar energy can dissociate water molecules into oxygen gas and a storable molecular H_2 .¹⁻⁴ Following light irradiation, the photogenerated holes diffuse to the semiconductor/electrolyte interface to strip the oxygen from the water (photooxidation) and the electrons migrate to the counter electrode to reduce the generated H^+ ions (H_2 -reduction). Consequently, the PEC-WS process is highly dependent on the carrier dynamic characteristics in the semiconductor photoelectrode, where a fast delivery of the photogenerated charge carriers to the water redox reaction interfaces is required.⁵ Among the semiconductor materials, the InGaN/GaN multi-quantum well coaxial nanowires (MQW-CNWs) are considered to be an efficient light harvesting medium with a tunable direct band gap energy that covers a large portion of the entire

solar spectrum.^{1,3,4,6} The growth of InGaN/GaN MQWs on the semipolar sidewall facets of GaN nanowires results in the reduced density of extended defects,⁷ a greater and more uniform In concentration,⁸ and mitigates the polarization-induced internal fields.⁹ Furthermore, the enhanced surface-to-volume ratio provided by the core-shell geometry can significantly increase the light capture and absorption as well as improve the collection efficiency of the photogenerated carriers.¹⁰ The photoanodes with nanoscale dimensions may also provide enhanced charge separation and increased quantum efficiency due to the significantly reduced travelling distance of the photogenerated carriers to the desired water redox reaction sites.^{10,11}

Whilst there has been extensive research and much progress in the development of InGaN-based structures to enhance the PEC-WS efficiency, there are no reports on the carrier dynamics of these structures and their impact upon the PEC-WS process.^{1,3,4,6} In InGaN/GaN structures the photogenerated charge carriers may have more complicated pathways that are in addition to separation and need to be carefully considered. For instance, in InGaN/GaN MQWs, the photogenerated carriers are preferably relaxed to the lower energy localized states created by In-rich nanoscale clusters formed through the In concentration fluctuation in the InGaN alloy.¹² As a result, the carrier diffusion length can be limited by the associated exciton localization effects. Furthermore, the defect-induced trapping states may act as alternative recombination channels for the photogenerated carriers, which leads to additional charge losses and significantly reduces the quantum efficiency of the PEC-WS process.¹³ Consequently, additional insight can be gained from a detailed study of the underlying processes that occur in the InGaN active medium and the influence on the PEC-WS performance. Here, we investigate the enhancement of the PEC-WS efficiency using a simple and high yield approach based on the quantum well (QW) engineering of InGaN/GaN MQW-CNWs. The current study may also provide a meaningful visualization for the carrier dynamics in the InGaN-based photoanodes and its impact on the relative H₂ generation photocurrent density (J_{ph}), which can significantly contribute on the deep understanding of

the artificial photosynthesis of water. A rational explanation of the influence of the exciton localization and the defect-induced recombination that can reduce the quantum efficiency of PEC-WS will be also given through this study.

Results and discussion

The photoelectrode used in the present study consists of InGaN/GaN MQW-CNWs synthesized on a c-plane sapphire substrate using a previously described two-step metalorganic chemical vapor deposition (MOCVD) growth.¹⁴ The light harvesting medium in this nanoscale architecture is composed of six pairs of InGaN/GaN MQW deposited coaxially on the semipolar sidewall facets of GaN nanowire templates with triangular cross-sections. Three samples, which have the same In composition, a variable QW thickness (1.5, 3.0 and 6.0 nm) and the same GaN barrier thickness of 9.6 nm, were grown and investigated. Figure 1(a) schematically shows the structure of a representative single nanowire composed of a GaN core covered radially with InGaN/GaN MQW shells. The as-grown MQW-CNWs had a high aspect ratio (~ 20) and a high density ($\sim 4.8 \pm 0.3 \mu\text{m}^{-2}$), as shown by the large scale tilted field emission scanning electron microscopy (FE-SEM) image in Fig. 1b. The microstructure and crystal quality of the MQW-CNWs were previously investigated using a high resolution scanning transmission electron microscopy (STEM) (JEM-2100F, JEOL Japan) with an accelerating voltage of 200 KeV and a point resolution of 0.10 nm.¹⁴ The sample with 3 nm QW was selected to be investigated using STEM. As schematically depicted in Fig. 1c, a thin GaN core was heterostructured with six InGaN/GaN MQW pairs that formed a nanoscale MQW structure with a superior surface-to-volume ratio. While the thickness was controlled by varying the growth time during the MOCVD growth, uniform thickness profiles of the GaN and InGaN layers can be clearly identified in the magnified STEM micrograph shown in Fig. 1d. The growth directions of the MQW were investigated using selective area electron diffraction (SAED) probed along a zone axis perpendicular to the growth direction of the investigated nanowire, which revealed the growth of MQW shells initially on the $\{1-101\}$ semipolar planes that was

altered to $\{2-201\}$ with increased number of QWs. No MQW growth was observed on the base of the GaN core, suggesting this plane to be the N-polar (000-1) plane. The high resolution lattice-resolved STEM images shown in Fig. 2e and 2f revealed the single crystallinity of the GaN core and the atomically sharp interfaces between the GaN and InGaN layers. A relatively high In composition of approximately 22% in the semipolar MQW structure was estimated using high resolution STEM spatial energy dispersive X-ray spectroscopy (EDX). A detailed microstructure characterization of the as-grown MQW-CNWs using STEM can be found in our recent publication.¹⁴

To investigate the impact of varying the InGaN QW thickness on the PEC performance of the MQW-CNWs, the as-grown samples were used as the photoanode in a homemade PEC cell designed with a two-electrode configuration where a Pt wire was used as the counter electrode. In a 1 M HCl water-based electrolyte, the MQW-CNWs were irradiated using simulated sunlight provided by a 300 W Xe lamp (Newport 66902) with a light irradiance of 150 mW cm^{-2} and an exposed area of approximately 0.5026 cm^2 . Following the light irradiation, the photogenerated electrons collected by GaN nanowire core are transported through the wetting layer at the bottom of the MQW-CNWs to In contact made on the sample surface. The In contact was connected to Pt counter electrode with conductive Cu wire. The linear sweeps of the J_{ph} , which are shown in Fig. 2a, revealed highly sensitive anodic behaviors to the InGaN QW thickness. H_2 generation was achieved immediately as the photoanode was irradiated with the simulated sunlight, which was visualized by plentiful amounts of H_2 gas bubbles that were evolved at the counter electrode. The initial response of the sample grown with the thinnest InGaN QW (1.5 nm) was delayed with a large onset potential of approximately 0.2 V. As the QW became thicker, a significant decrease of the onset potential and a greater J_{ph} were achieved. While the large onset potential is dominant for the samples grown with 1.5 and 3.0 nm QWs, at 6.0 nm, the onset potential was significantly reduced to -0.32 V, which contributed to a greater J_{ph} of 2.3 mA cm^{-2} at 1.1 V and a 0.6 mA cm^{-2} at zero bias. Achieving a low onset potential is extremely important because it reduces the applied

bias required to attain the maximum photocurrent and, hence, increases the overall efficiency of the PEC-WS. The negative onset potential and the high zero-bias J_{ph} of the sample with 6 nm QW demonstrates the ability of the MQW-CNWs for splitting water and producing H_2 fuel with sunlight being the only external energy input. To investigate the contributions of GaN and InGaN layers to the light absorption and to evaluate the photoactivity of the photoanode, the incident-photon-to-current conversion efficiency (IPCE) was measured as a function of the QW thickness, as shown in Fig. 2b. The IPCE (the external quantum efficiency) is a measure of the ratio of the number of photogenerated electrons taking part in the redox reactions to the number of incident monochromatic photons as a function of the wavelength. The IPCE was calculated from equation (1):³

$$IPCE (\%) = \frac{1240 \times J_{ph} (mAcm^{-2})}{\lambda (nm) \times P_{light} (mWcm^{-2})} \times 100$$

(1)

where λ is the wavelength of the monochromatic photons and P_{light} is the power density of the light at a given wavelength. As the QW was thick enough (6.0 nm) and subject to UV irradiation where the carriers in both the GaN and InGaN layers can be excited, the IPCE attained a maximum of 15%, which was reduced by thinning the QW. From Fig. 2a and 2b, it can be concluded that a thick QW (active region) in semipolar InGaN-based heterostructures is necessary to improve their photoactivity and to promote the quantum efficiency. To further elucidate the performance of the MQW-CNWs as a function of the QW thickness, we measured the applied bias photon-to-current efficiency (ABPE), which can provide diagnostic measurements that represent the development of the photoanode performance with respect to the applied potential. The ABPE was measured from equation (2):¹⁵

$$ABPE (\%) = \frac{J_{ph} (mAcm^{-2}) \times (1.4 - V_{app} (V))}{P_{light} (mWcm^{-2})} \times 100$$

where 1.4 V is the standard state reversible potential of Cl^- instead of that of water because we used HCl electrolyte¹⁶ and V_{app} is the applied potential during the measurement. As shown in Fig. 2c, with an

increased QW thickness, the optimal potential representing the best performance of the PEC cell shifted to lower values, which indicates an interesting modification of the photoanodic performance with widening the QW.

To understand the improved PEC-WS performance in the case of the thick QW, the emission properties of two single nanowires with different QW thicknesses of 1.5 and 6 nm were scanned spatially along their axes using room temperature cathodoluminescence (CL) (Gatan, Mono CL4) with an accelerating voltage of 3 keV and a step size of approximately 2 nm. To investigate the spatially resolved CL, the as-grown nanowires were detached from the sapphire substrate and dispersed on a cleaned Si-wafer where they can precisely selected. The spatial excitation of a single nanowires may provide meaningful characteristics of the photoemission and, hence, the optical band gap, which are critical parameters that determine the photoactivity of the semiconductor photoanode. The CL line-scan mapping images depicted in Fig. 3a and 3b revealed distinct emission profiles with respect to the QW thickness. A clear GaN-related signal and a broad emission that extended to the defect-related yellow luminescence were detected from the nanowire with the thin QW (1.5 nm). Conversely, a strong band-to-band emission was observed with an increased QW thickness (6 nm) without any signal from the GaN, which suggests high optical qualities and well-coated GaN nanowire cores. The obtained CL line-scan mapping images can be further explained by the resolved CL spectra collected in Fig. 3c and 3d, which were selected to show the evolution of the CL emission along the nanowire axis. Broad emissions combined with the GaN peak were detected along the axis of the nanowire with a thin QW; however, the nanowire with a 6 nm QW showed narrow emission peaks without GaN signals or defect-related yellow luminescence. The observed peak broadening at longer wavelengths in the case of the thin QW can be explained on the bases of the associated structural imperfections. In the very thin InGaIn layer, several crystal defects may occur, such as In segregation, interfacial roughness, and solid-state intermixing between the InN and GaN that can lead to a significant In fluctuation in the QW.^{17,18} Furthermore, the

thin InGaN QW could allow the photogenerated carriers to escape and recombine through the defect states of the underlying and capping GaN layers, which can also contribute to the CL peak broadening. The outstanding photoemission profile demonstrated by the nanowire with a 6 nm QW thickness may explain the improved PEC-WS performance of the MQW-CNWs photoanode with a thick QW.

The photoemission characteristics were further investigated by the room temperature photoluminescence (PL) and the time-resolved PL (TRPL) spectroscopies as a function of the QW thickness. For the room temperature PL, the samples were excited using a 325 nm continuous-wave He-Cd laser with an average optical power of 10 mW, and a Ti:sapphire pulsed laser with a small optical power of approximately 10 μ W was employed as the excitation source in the TRPL measurements. The PL decays were detected by a streak camera (Hamamatsu, C7700-01) with a time resolution less than 300 fs and a repetition rate of approximately 4 MHz. The excitation wavelength of the Ti:sapphire pulsed laser was tuned at 400 nm to selectively excite the InGaN QW only. The room temperature PL and TRPL spectra, as shown in Fig. 4a and 4b, revealed that the carrier dynamics of the MQW-CNWs are highly dependent on the InGaN QW thickness. Consistent with the CL results, the room temperature PL spectra revealed an improved photoemission quality with an increase in the QW thickness, and the PL of the thin QW sample was governed with a clear defect-related yellow emission. The PL decay curves shown in Fig. 4b can give an overall view of the QW thickness-dependent carrier dynamics of the as-grown MQW-CNWs. All decay curves exhibited a non-exponential decay profile, which can be attributed to the In concentration fluctuation within the InGaN alloy.¹⁹ Recently, the stretched exponential decay model has been accepted to adequately explain such TRPL decays from InGaN-based structures under a variety of condition.¹⁹⁻²¹ Therefore, the observed PL decays were fitted using the stretched exponential function given by equation (3):

$$I(t) = I(0) \exp\left[-(t/\tau)^\beta\right]$$

(3)

where $I(t)$ is the PL intensity at a decay time t , $I(0)$ is the initial PL intensity, β is the stretching parameter related to the In fluctuation in the InGaN alloy, and τ is the initial lifetime at the greatest carrier density. The β and τ values can be determined through a linear fitting of the plot of the double logarithm of the PL decay versus the natural logarithm of the decay time, as shown in Fig. 4c-4e. The estimated β and τ values for all samples are listed in Table 1. The radiative and non-radiative recombination lifetimes (namely τ_{rad} and τ_{non} , respectively) can be then calculated by solving the equations $IQE = (1 + \tau_{rad} / \tau_{non})^{-1}$ & $1/\tau = 1/\tau_{rad} + 1/\tau_{non}$.¹⁹ The IQE (the ratio between the PL peak intensity at 300 K and 10 K, assuming the freeze-out of the defect-induced non-radiative recombination at extremely low temperature) was measured from the Arrhenius plot representing the variation of the integrated PL intensity as a function of the temperature, as shown in Fig. 5a. To investigate the temperature-dependent variation of the PL intensity with respect to the QW thickness, the samples were mounted in a closed-cycle He cryostat and the temperature was controlled from 10 to 300 K. The integrated PL intensity of the investigated samples showed a good saturation up to 100 K and then a gradual degradation depending on the QW thickness. The sample grown with a 6 nm QW exhibited the greatest IQE of 54.7 %, which is about two times greater than the IQE of a comparable planar semipolar MQW structure.⁹ The τ_{rad} and τ_{non} were then calculated using the values estimated for IQE and τ , as shown in Table 1. The investigated samples showed ultrafast carrier dynamics in the range of several tens to a few hundred ps, which is consistent with the reported lifetimes of similar semipolar MQW structures.²² In the c-plane MQWs, the quantum-confined Stark effect (QCSE) induced by the piezoelectric and polarization fields significantly tilt the energy bands of the QW and separate the electron and hole wave functions leading to increased charge separation and longer lifetimes.²³ In contrast, the nanoscale semipolar MQWs showed reduced or even negligible internal fields.^{22,23} Consequently, the energy bands of the semipolar MQWs are almost flat, and the internal fields have minor effects on the carrier dynamics. Meanwhile, faster carrier transitions and shorter lifetimes are

expected. As shown in Table 1, τ_{rad} was significantly reduced with an increase in the QW thickness, and at 6 nm τ_{rad} was approximately nine times shorter than τ_{rad} with the 1.5 nm QW sample. Furthermore, in the case of a 6 nm QW τ_{rad} was exclusively shorter than τ_{non} , which indicates an improved crystal quality and a reduced In fluctuation at this QW thickness. The long time needed for the excited carriers to recombine through the radiative recombination channels at the very thin QW (1.5 nm) suggests that the carrier lifetime was limited by a combination of many mechanisms.

Because in InGaN/GaN MQW structures the free excitons tend to relax to the localized states (the lowest energy states),¹² the exciton localization effects can also be a major parameter that affects the carrier lifetime of the photogenerated charge carriers. The temperature-dependent variation of the PL peak energy can explain the exciton localization mechanism as a function of the QW thickness, which assumes that the density of the states in the conduction and the valence bands follow a Gaussian-like distribution. The temperature-dependent variations of the emission energy, as shown in Fig. 5b-d, can give an overall view of the degree of exciton localization with respect to the QW thickness. We observed a distinct temperature dependency of the emission energy with respect to the QW thickness. Up to 3 nm, the emission energy can be described by the common S-like-shaped profile; however, as the QW become thick enough (6 nm), the emission energy decreased monotonically with the temperature. The observed S-shaped profile of the emission energy was accepted to originate from the localized tail states induced by the inhomogeneous In distribution in the InGaN QW.²⁴ The inhomogeneous distribution of In atoms in the InGaN alloy can lead to a local potential fluctuation (potential minima) that may act as a carrier trap states in the same QW, which is known as lateral confinement.²⁵ For comparison, the temperature-dependent variation of the PL peak energy was fitted using a Varshni model, which is given by equation (4):⁹

$$E(T) = E_g(0) - \frac{\alpha T^2}{T + \beta} \quad (4)$$

where $E(T)$ is the emission energy at temperature (T), $E_g(0)$ is the energy gap at 0 K, and α and β are Varshni's fitting parameters. With an increase in the QW thickness, the dependence of the PL emission energy on the temperature was increased, and at 6 nm, the emission energy can be well fitted by the Varshni model. The absence of the S-like-shaped variation in the PL peak energy and a good fit using the Varshni model at 6 nm suggests negligible localization effects.²⁶ The fact that the thermal activation energy (E_a) is equivalent to the depth of the confining potential minima, which is the energy needed by the localized carriers to thermally escape from their localized states, also gives meaningful insight into the localization degree as a function of the QW thickness. The E_a was estimated from the slope of the Arrhenius plots, as shown in Fig. 5a, in the high temperature range where the thermal quenching process is the major parameter affecting the carrier dynamics. The estimated values of E_a , as shown in Table 1, revealed that the exciton localization was significantly reduced with an increase in the QW thickness, which may also explain the observed decrease of the carrier lifetime obtained by the TRPL analysis. From the values of τ_{rad} , IQE, and E_a , we may conclude that the exciton localization effects and the defect-induced recombination can play an important role in the carrier dynamics up to a critical QW thickness (3 nm in this case), which will be insignificant in wider QWs. These findings, together with the presented PEC-WS performances shown Fig. 2, allow us to develop a general model for the carrier dynamics in the semipolar MQW-based photoanode and its role in the PEC-WS process with respect to the QW thickness.

In general, the overall PEC-WS process can be defined by a series of successive mechanisms, as shown in Fig. 6, starting from the light excitation followed by the photogeneration of electron-hole pairs, the charge separation, the charge transportation to the desired redox reaction interfaces, and the photooxidation and H_2 -reduction half-reactions. However, the dynamics of the photogenerated carriers in the pre-excited semiconductor photoelectrode are the key parameters that influence the overall PEC-WS efficiency, which is different in the time scale from the in situ carrier kinetics during the PEC-WS

process. In this study, we observed a strong relation between the QW thickness and the crystal quality as well as the optical characteristics of the MQW-CNWs, which can significantly affect the carrier dynamics in the photoelectrode and, hence, the carrier kinetics during the PEC-WS process. It was demonstrated in this study that the carrier dynamics in the case of thin QWs are ruled by two mechanisms: the exciton localization and the defect-induced recombination. The former mechanism can lead to a lateral confinement effects that can effectively reduce the diffusion length of the photogenerated carriers, and the additional recombination channels made by the latter mechanism may lead to a significant carrier loss, as shown in Fig. 6b. Both mechanisms can reduce the supply rate of photogenerated carriers to the desired water redox reaction sites and slow down the photooxidation and H₂-reduction processes. As a result, a large overpotential is needed to artificially start the PEC-WS process, which can be demonstrated by the large onset potential observed in the case of the thin QW samples (Fig. 2a). Conversely, the weak localization and the improved crystal quality (low defect density), which is shown by the thick QW sample (6 nm), can increase the carrier diffusion length and improve the carrier transportation to the desired interfaces, which results in a smaller onset potential and greater conversion efficiencies. The weak localization and the improved crystal quality may also provide a greater density of charge carriers that participate at the NW/electrolyte interface, which can significantly improve the driving force for H₂ evolution.

Conclusions

In summary, the carrier dynamics of InGaN/GaN MQW-CNWs were studied in detail using different PL spectroscopies including room temperature, time-resolved and temperature-dependent methods as a function of the QW thickness. The results revealed a strong dependency of the carrier dynamics and the crystal quality on the QW thickness. Defect-related recombination and strong exciton localization were observed in samples with thin QWs, whereas strong band-to-band transitions and negligible localization were demonstrated by the thick QW sample. With respect to carrier dynamics, the PEC-WS efficiency,

in the case of thin QWs, can be limited by carrier localization and by defect-induced recombination, which may significantly reduce the carrier diffusion length and increase the charge loss. As a result, the efficient InGaN-based photoanode requires high crystal quality and small exciton localization, which can be achieved through careful structural optimization. Following this approach, a high IPCE of approximately 15% and a high zero-bias J_{ph} were achieved by engineering the QWs in the MQW-CNWs photoanode, which can potentially pave the way for integrating InGaN-based heterostructure nanowires in solar H_2 generation technology.

Acknowledgments

This work was supported by the National Research Foundation of Korea (NRF) Grant funded by the Korean Government (NRF-2013R1A1A2059179).

Notes and references

1. B. AlOtaibi, H. P. T. Nguyen, S. Zhao, M. G. Kibria, S. Fan and Z. Mi, *Nano Lett.*, 2013, 13, 4356.
2. G. Wang, H. Wang, Y. Ling, Y. Tang, X. Yang, R. C. Fitzmorris, C. Wang, J. Z. Zhang and Y. Li, *Nano Lett.*, 2011, 11, 3026.
3. W. Luo, B. Liu, Z. Li, Z. Xie, D. Chen, Z. Zou and R. Zhang, *Appl. Phys. Lett.*, 2008, 92, 262110.
4. N. H. Alvi, P. E. D. S. Rodriguez, P. Kumar, V. J. Gomez, P. Aseev, A. H. Alvi, M. A. Alvi, M. Willander and R. Notzel, *Appl. Phys. Lett.*, 2014, 104, 223104.
5. J. B. Baxter, C. Richter and C. A. Schmuttenmaer, *Annu. Rev. Phys. Chem.*, 2014, 65, 423.
6. R. Dahal, B. N. Panth, J. Li, J. Y. Lin and H. X. Jiang, *Appl. Phys. Lett.*, 2014, 104, 143901.
7. M. Hugues, P. A. Shields, F. Sacconi, M. Mexis, M. Auf der Maur, M. Cooke, M. Dineen, A. Di Carlo, D. W. E. Allsopp and J. Zuniga-Perez, *J. Appl. Phys.*, 2013, 114, 084307.
8. T. Kuykendall, P. Ulrich, S. Aloni and P. Yang, *Nat. Mater.*, 2007, 6, 951.
9. H. Yu, L. K. Lee, T. Jung and P. C. Ku, *Appl. Phys. Lett.*, 2007, 90, 141906.
10. J. Ji, W. Zhang, H. Zhang, Y. Qiu, Y. Wang, Y. Luo and L. Hu, *J. Mater. Sci. Mater. Electron.*, 2013, 24, 3474.
11. J. M. Foley, M. J. Price, J. I. Feldblyum S. Maldonado, *Energy Environ. Sci.*, 2012, 5, 5203.
12. J. H. Na, R. A. Taylor and K. H. Lee, *Appl. Phys. Lett.*, 2006, 89, 253120.
13. S. F. Chichibu, A. Uedono, T. Onuma, B. A. Haskell, A. Chakraborty, T. Koyama, P. T. Fini, S. Keller, S. P. Denbaars, J. S. Speck, U. K. Mishra, S. Nakamura, S. Yamaguchi, S. Kamiyama, H. Amano, I. Akasaki, J. Han and T. Sota, *Nat. Mater.*, 2006, 5, 810.

14. M. Ebaid, J. H. Kang, S. H. Lim, J. S. Ha, J. K. Lee, Y. H. Cho, and S. W. Ryu, , *Nano Energy*, 2015, in press. <http://dx.doi.org/10.1016/j.nanoen.2014.12.033>.
15. I. Fujimoto, N. Wang, R. Saito, Y. Miseki, T. Gunji and K. Sayama, *Int. J. Hydrogen Energy*, 2014, 39, 2454.
16. M. Ono, K. Fujii, T. Ito, Y. Iwaki, A. Hirako, T. Yao, and K. Ohkawa, *J. Chem. Phys.*, 2007, 126, 054708.
17. S. Y. Kwon, H. J. Kim, E. Yoon, Y. Jang, K. J. Yee, D. Lee, S. H. Park, D. Y. Park, H. Cheong and F. Ro, *J. Appl. Phys.*, 2008, 103, 063509.
18. S. M. Ko, H. S. Kwack, C. Park, Y. S. Yoo, S. Y. Kwon, H. J. Kim, E. Yoon, L. S. Dang and Y. H. Cho, *Appl. Phys. Lett.*, 2013, 103, 222104.
19. M. Ebaid, J. H. Kang, S. H. Lim, S. M. Ko, Y. H. Cho and S. W. Ryu, *Acta Mater.*, 2014, 65, 118.
20. B. Jiang, C. Zhang, X. Wang, F. Xue, M. J. Park, J. S. Kwak and M. Xiao, *Opt. Express*, 2012, 20, 13478.
21. D. Li, X. Dong, J. Huang, X. Liu, Z. Xu, X. Wang, Z. Zhang and Z. Wang, *J. Cryst. Growth*, 2003, 249, 72.
22. M. Ueda, K. Kojima, M. Funato, Y. Kawakami, Y. Narukawa and T. Mukai, *Appl. Phys. Lett.*, 2006, 89, 211907.
23. Y. Ji, W. Liu, T. Erdem, R. Chen, S. T. Tan, Z. H. Zhang, Z. Ju, X. Zhang, H. Sun, X. W. Sun, Y. Zhao, S. P. DenBaars, S. Nakamura and H. V. Demir, *Appl. Phys. Lett.*, 2014, 104, 143506.
24. Y. H. Cho, G. H. Gainer, A. J. Fischer, J. J. Song, S. Keller, U. K. Mishra and S. P. DenBaars, *Appl. Phys. Lett.*, 1998, 73, 1370.
25. C. Shi, C. Zhang, F. Yang, M. J. Park, J. S. Kwak, S. Jung, Y. H. Choi, X. Wang and M. Xiao, *Opt. Express*, 2014, 22, A790.
26. J. Bai, T. Wang and S. Sakai, *J. Appl. Phys.*, 2000, 88, 4729.

Table 1. TRPL fitting parameters estimated by the stretched exponential model as a function of the InGaN QW thickness and the thermal activation energy (E_a) as estimated from the slope of the high temperature range in the Arrhenius plots shown in Fig. 5a.

QW thickness (nm)	β	τ (ps)	τ_{rad} (ps)	τ_{non} (ps)	E_a (meV)
1.5	0.49	78.8	469.1	94.8	11.3
3.0	0.59	38.9	122.7	57.1	6.1
6.0	0.64	28.8	52.7	63.4	4.6

Figure Captions

Fig. 1. (a) Schematic diagram showing the structure of a single InGaN/GaN MQW-CNW. (b) Large scale FE-SEM tilted image showing the morphology of the as-grown MQW-CNWs. (c) Schematic representation of the cross-sectional view of the MQW-CNWs. (d) Magnified view of the selected zone highlighted in (c), which shows the six pairs of the MQW shell. (e) Lattice-resolved STEM image showing the single crystallinity of the GaN core. (f) Lattice-resolved STEM image showing the sharp and smooth interfaces between GaN and InGaN layers.

Fig. 2. (a) Linear sweeps of J_{ph} as a function of the QW thickness. (b) The measured IPCE with respect to the QW thickness that was measured using monochromatic photons obtained using band-pass optical filters of specific wavelengths. (c) The ABPE as a function of the QW thickness.

Fig. 3. The CL line-scan mapping of a single MQW-CNW with QW thicknesses of (a) 1.5 nm and (b) 6.0 nm. (c) The resolved CL spectra of the selected spots in (a). (d) The resolved CL spectra of the selected spots in (b).

Fig. 4. (a) Room temperature PL of the as-grown InGaN/GaN MQW-CNWs. (b) TRPL decay curves as a function of the QW thickness. The instrumental response function (IRF) of the TRPL setup is also included as the green open circles. (c)-(e) The stretched exponential fit of the decay curves shown in (b), which were used for the estimation of τ and β values.

Fig. 5. (a) The IQE of MQW-CNWs as measured from the Arrhenius plots of the temperature-dependent variation of the integrated PL intensity as a function of the QW thickness. (b)-(d) The temperature-dependent variation of the PL peak energy and the corresponding Varshni model fitting.

Fig. 6. Schematic illustrations showing the concept of the PEC-WS process using MQW-CNW photoanode. A single QW structure was shown for simplicity. (a) Various mechanisms occur during the PEC-WS process including: (I) light excitation, (II) photogeneration of electron-hole pairs, (III) charge separation, (IV) charge transportation to the desired redox reactions interfaces, and (V) photooxidation and H_2 -reduction reactions. (b) A magnified view of the case of a thin QW showing the lateral confinement and the defect-induced non-radiative recombination mechanisms.

Fig. 1

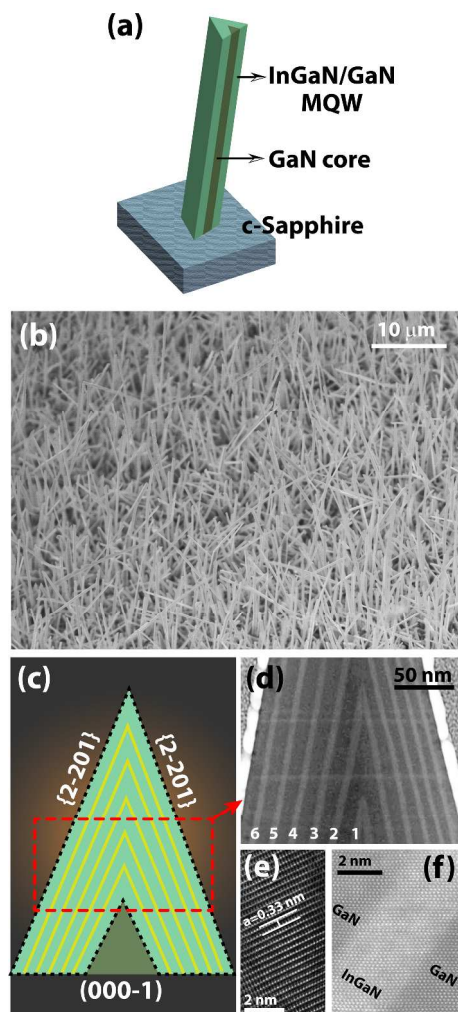


Fig. 2

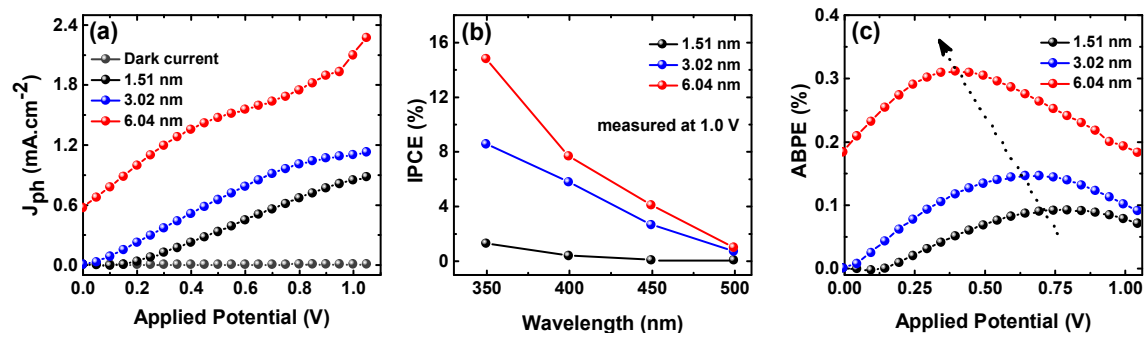


Fig. 3

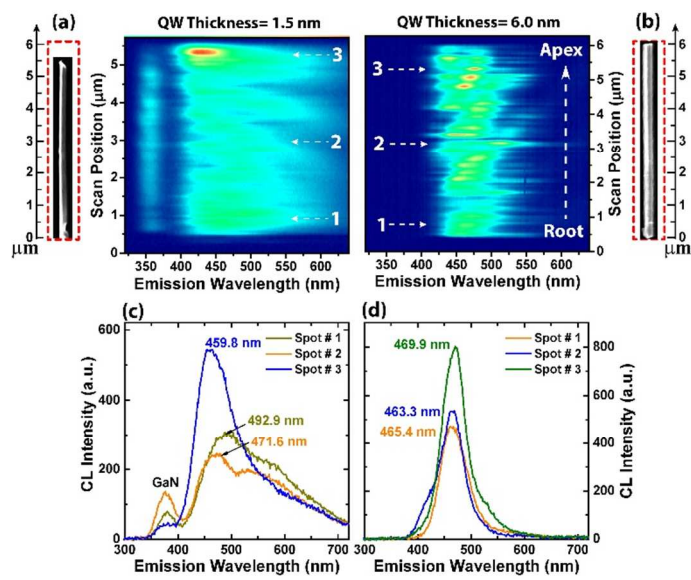


Fig. 4

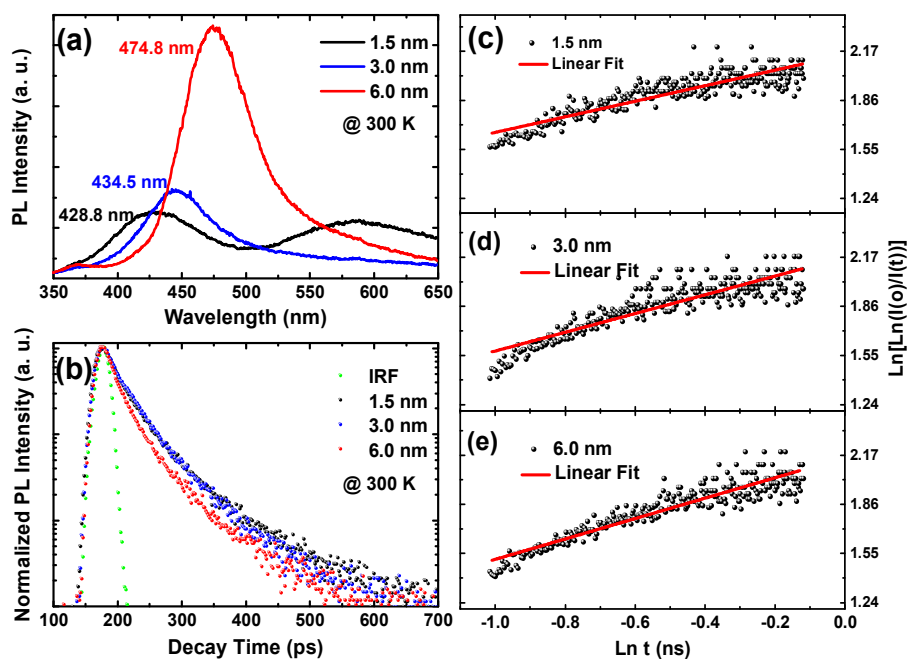


Fig. 5

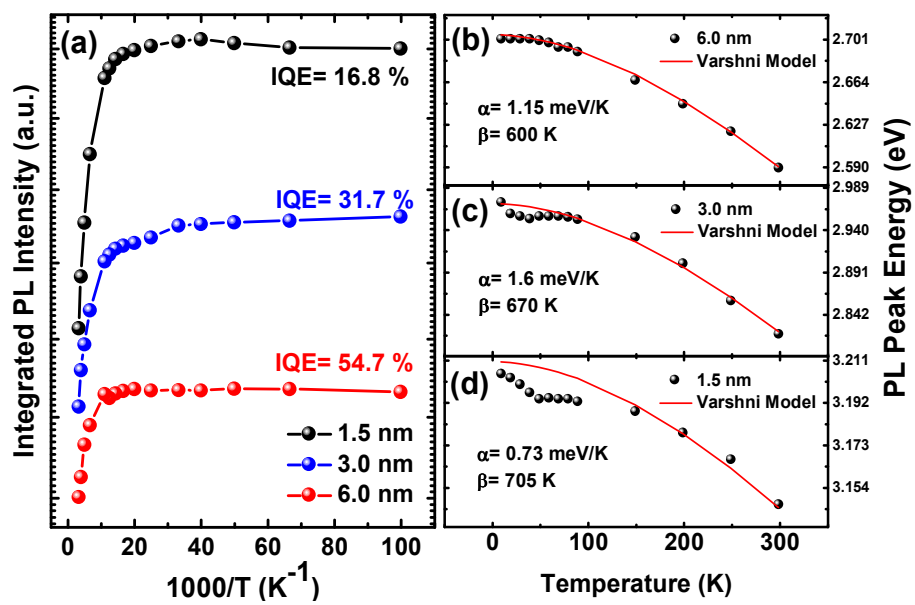


Fig. 6

